Variance and spectra of fluorescence-intensity fluctuations from two-level atoms in a phase-diffusing field

M. H. Anderson, R. D. Jones, J. Cooper, and S. J. Smith
Joint Institute for Laboratory Astrophysics, University of Colorado and National Institute of Standards and Technology, Boulder, Colorado 80309-0440

D. S. Elliott
School of Electrical Engineering, Purdue University, West Lafayette, Indiana 47907

H. Ritsch and P. Zoller
Institute for Theoretical Physics, University of Innsbruck, A-6020 Innsbruck, Austria
(Received 23 April 1990)

We have measured the variance in fluorescence intensity and the spectrum of those fluctuations for two-level atoms in a phase-diffusing laser field. We compare our results with recent theoretical predictions that have been extended to include the effects of Doppler broadening and spatial variation of the laser intensity. Our study includes the effects of laser power, bandwidth, and shape (Lorentzian and non-Lorentzian) of the laser spectrum. At lower laser intensities, our measured variances versus detuning are in quantitative agreement with the theoretical predictions. At intensities above saturation, the variance is sensitive to inhomogeneities in the distribution of laser intensity in the interaction region, and only qualitative agreement is achieved. Asymmetries in the variance versus detuning resulting from correlated amplitude and phase noise have been observed. Spectra of the phase-noise-induced fluorescence-intensity fluctuations are shown to contain contributions from transients excited by the phase noise and are more sensitive to artifacts in the noise modulation process than the intensity spectrum of the laser field itself.

I. INTRODUCTION

In the field of precision measurements the observed quantity is often derived from the fluorescence of an atomic transition. Recently, it has been noticed that fluctuations in the fluorescence from atoms driven by a laser field have a nontrivial dependence on the laser detuning and can dominate the background noise level.[1] Haslwanter *et al.*[2] and Ritsch, Zoller, and Cooper[3] have shown that such fluctuations may derive from phase and/or amplitude fluctuations of the driving laser field. Since fluorescence-intensity fluctuations can set a limit on the experimental resolution, it is of practical importance to understand the effects of different statistical models for laser light on the variance of the fluorescence intensity. In a previous article[4] we presented some results of an investigation, inspired by these observations,[1] on the variance of fluorescence-intensity fluctuations. The present paper presents the detailed results from a comprehensive experimental investigation of the variance and spectrum of fluorescence-intensity fluctuations from a large number of two-level atoms driven by a phase-diffusing laser field, and it also presents a quantitative comparison of these results to theoretical calculations. The variance and spectrum of fluorescence-intensity fluctuations are shown to depend on the magnitude and time scale of the phase fluctuations, the laser intensity, and the laser detuning. Our analysis also accounts for experimental conditions such as Doppler broadening, the laser-intensity distribution across the interaction region, and the time response of the detector.

It is known that single-atom quantum effects and the mutual coherence of the fluorescence can affect correlations in the fluorescence intensity.[5] For a very small number of atoms, quantum effects give rise to photon antibunching. For a large number of atoms, but with a small detector, the fluorescence becomes characteristic of thermal statistics and exhibits photon bunching. The work in this paper considers the case of fluorescence emitted from a large number atoms (approximately 10^5) and measured with a detector with an area much larger than the coherence area of the fluorescence. Under these conditions the effects mentioned above are small, and the intensity fluctuations are related to population fluctuations of the upper state of the individual atoms.[3] The effects that we measure are purely classical.

The observables in this experiment are the time-averaged fluorescence intensity $\langle I(t)\rangle$, its variance $[\Delta I(t)]^2 \equiv \langle I(t)^2\rangle - \langle I(t)\rangle^2$, and also the spectrum of the intensity fluctuations $P_I(\omega)$. By the Wiener-Khintchine theorem, $P_I(\omega)$ is dependent on the Fourier transform of the intensity autocorrelation function $\langle I(t)I(t+\tau)\rangle$. Classically, this can also be written as $\langle E(t)E^*(t)E(t+\tau)E^*(t+\tau)\rangle$, which is a fourth-order correlation of the electric field at the detector, and depends on a summation of fields emitted by different atoms in the interaction region.

The theoretical aspects of intensity correlations in the

fluorescence from atoms driven by fluctuating laser fields have been considered by several authors. Much of the previous literature is concerned with the effect of fluctuating laser fields on the intensity correlations from a single atom giving rise to photon antibunching.[6] Intensity correlations, related to the correlations in the upper-state population of many two-level atoms, have only recently received attention.[2,3,7] In the work of Rzazewski, Stone, and Wilkens[7] the two-time intensity autocorrelation function was derived in the weak-field limit for both the phase diffusing and chaotic fields. The transform of the two-time intensity autocorrelation function was calculated in Ref. 7, giving an expression for the spectrum of the intensity fluctuations in the weak-field limit. The work of Haslwanter *et al.*[2] used a density-matrix formalism to arrive at a set of stochastic differential equations valid for both low and high intensities. These differential equations are averaged over the phase fluctuations and then solved for the variance of the upper-state population. Two statistical models of the laser field are considered: the phase-diffusion model (PDM), and a phase-jump model (PJM). This theory was extended by Ritsch, Zoller, and Cooper[3] to include non-Lorentzian phase-diffusing fields with both correlated and uncorrelated amplitude fluctuations. The spectrum of the intensity fluctuation was also calculated in Ref. 3 and was shown to contain interesting features in the saturation regime. In this work, we compare our results with calculations based on the methods of Refs. 2 and 3. In a related work, Ferguson and Elliott[8] calculated the variance and spectrum of intensity fluctuations on the output of a Fabry-Pérot interferometer for phase-diffusing, chaotic, and real Gaussian fields. A high-finesse Fabry-Pérot interferometer is also considered briefly in Ref. 2, and was shown to behave like a large number of two-level atoms in the weak-field limit.

Many statistical models of the laser field have identical second-order field correlations. Hence the intensity spectrum of the laser field $P_E(\omega)$, given by the transform of the second-order field correlation, will also be identical. In the weak-field limit, $\langle I(t)I(t+\tau)\rangle$ is ultimately related to integrals of fourth-order correlations of the input field. As a result, our observable, the variance of the fluorescence intensity, is sensitive to differences between different statistical models of the laser fields even in weak fields. For example, it is shown in Ref. 2 that the variance is particularly sensitive to differences between the PDM and PJM in the low-field limit. In addition to the dependence on fourth-order correlations, it is the frequency dependence of the atomic resonances that makes the variance in the fluorescence intensity particularly sensitive to different statistical models of the frequency or phase. Experiments are in progress to measure the variance of the fluorescence intensity from atoms driven by phase-jump fields.[9]

The weak-field dependence on fourth-order field correlations, as in this work, is in contrast with some previous experiments that investigated the Autler-Townes effect and the Hanle effect in the presence of phase-diffusing fields.[10,11] In these other experiments, the observable depended on second-order field correlations in the weak-field limit and did not depend on higher-order correlations unless the laser field was saturating. However, the variance of the fluorescence intensity is not unique in its dependence on higher-order statistics of the input field. For example, observables in the field of optical coherent transients also depend on higher-order statistics of the input field.[12,13] That work differs from ours in the particular correlation functions and the integrals over time which determine the manner in which they are related to the observable.

Besides the coherent transients experiments, there are others which also can, in principle, measure higher-order correlations of the input field. For example, a previous experiment[14] investigated the effects of two counterpropagating phase-diffusing lasers used to drive a two-photon transition in atomic sodium. The absorption of two photons is related to fourth-order correlations of the input field in the weak-field limit (since the process is second order). This was demonstrated by a reduction in the absorption linewidth as the two fluctuating laser fields became decorrelated. Two-photon absorption should also distinguish between different statistical models of the laser field (which give identical laser spectra), and experiments in two-photon absorption are now being planned for phase-jump fields.[9] In a recent related experiment, Boscaino and Mantegna[15] observed the spectrum of the fluorescence for a two-photon transition in the microwave regime. They observed a marked difference between phase-jump and phase-diffusing fields even though these fields had identical second-order field correlation and, therefore, field spectra.

It is shown in Ref. 2 that for a low-intensity phase-diffusing laser with a spectral width less than the natural linewidth of the transition κ, the fluorescence intensity fluctuations $\Delta I(t)\equiv\{[\Delta I(t)]^2\}^{1/2}$ exhibit a double-peaked structure. This profile is a maximum at the laser detunings where the fluorescence profile has a maximum slope and is a minimum at zero detuning where the slope is zero. The structure in the profile can be explained with simple physical arguments. For simplicity we ignore effects such as Dopper broadening. A phase-diffusing laser can be considered as an "instantaneously" monochromatic laser undergoing small frequency (phase) perturbations. If the detuning of the laser is initially on resonance with the atoms, than any frequency perturbation will momentarily put the laser off resonance, resulting in a small decrease in the intensity of the resonance fluorescence. However, when the laser is tuned to the point of the emission profile where the slope is greatest, the changes in the fluorescence intensity will be larger than at zero detuning since the laser is most sensitive to the laser frequency at this point. This argument is valid for slow fluctuations that are less than the lifetime of the upper state τ. For faster fluctuations, a proper theoretical model must take the dynamics of the atom-field interaction into account, as in Refs. 2 and 5.

Similar arguments can be applied to the spectrum of the intensity fluctuations obtained from $\langle I(t)I(t+\tau)\rangle$. The optical Bloch equations, which describe the time evolution of a two-level atom, have three roots: one at $\omega=0$ and two others at $\omega=\pm\Omega'$. In this expression, Ω' is

the generalized Rabi frequency given by $\Omega'=(\Omega^2+\Delta^2)^{1/2}$, where Δ is the laser detuning from resonance and Ω is the zero detuning Rabi frequency. These roots each give rise to transients in the response of the atom that oscillate at the frequency of the root and are damped at a rate given by $\exp(-\kappa t)$, where $\kappa=1/\tau$ is the natural linewidth of the transition. The effect of the root at $\omega=0$ is to reduce the response of the atoms to frequency fluctuations on a time scale faster than τ, so the spectrum can be expected to contain a peak at $\omega=0$ and drop off at frequencies greater than κ. However, transients can also contribute to the spectrum of the intensity fluctuations at Ω'. This can best be illustrated with the example of optical nutation in which the atoms are exposed to a step pulsed laser field. After the onset of the laser field the fluorescence will be modulated at Ω' and damp out to a steady-state value. Recently, elegant experiments have been performed to observe this phenomenon.[16] However, if the atoms are exposed to a train of pulses or if the light is randomly modulated with a frequency range spanning Ω', then these transients are continuously excited and never completely damp out, thus contributing a side peak to the spectrum of the intensity fluctuations at Ω' with a width dependent on κ. The effect of phase fluctuations reinitiating transient responses in the atom, even in the steady state, has been noted by Knight, Molander, and Stroud.[17] For monochromatic excitation Ω' has a well-defined value, but for a phase-diffusing field the fluctuations in Δ effectively broaden Ω' and the width of the peak will also depend on the linewidth of the laser field. In Ref. 7 it is shown that the weak-field spectrum of intensity fluctuations consists of a peak centered at $\omega=0$ with a width of 2κ, and with side peaks [each of equal height since $P_I(\omega)=P_I(-\omega)$] centered at $\omega=\pm\Delta$ with a width of $\kappa+2b$, where $2b$ is the full width at half maximum (FWHM) of the laser field for the PDM. Although in the weak-field limit the side peaks are comparable to the central peak, they are difficult to observe because the overall fluorescence intensity is low at detunings where they become resolved from the central peak.

II. THEORETICAL BACKGROUND

We begin this section with a summary of the model for a phase-diffusing laser field. The laser field

$$E(\mathbf{x}_k(t),t)=\tfrac{1}{2}E(t)\exp\{-i[\omega_L t-\mathbf{k}\cdot\mathbf{x}_k(t)]\}+\text{c.c.}\ , \quad (1)$$

with

$$E(t)=E_0\exp[-i\phi(t)]\ ,$$

is assumed to have a constant amplitude E_0, and the phase $\phi(t)$ is assumed to be a Gaussian random variable analogous to the position of a particle undergoing Brownian motion. The spatial factor $\exp[i\mathbf{k}\cdot\mathbf{x}_k(t)]$ determines the field at the position of the kth atom and the time dependence in $\mathbf{x}_k(t)$ includes the possibility that the atom is moving. The stochastic frequency $\omega(t)=\dot{\phi}(t)$ is a Gaussian random variable with the correlation function assumed to be of the form[18]

$$\langle\omega(t)\omega(t+\tau)\rangle=b\beta\exp(-\beta|\tau|)\ , \quad (2)$$

where $b\beta$ is the variance of the frequency fluctuations and $1/\beta$ is the time scale of the fluctuations. The power spectrum of the frequency fluctuations is given by the Fourier transform of Eq. (2) with respect to τ,

$$P_\omega(\omega)=2b[1+(\omega/\beta)^2]^{-1}\ . \quad (3)$$

The laser field modeled in this way is referred to as the Brownian motion phase-diffusion model (BMPDM). For the case that $\beta\to\infty$, $P_\omega(\omega)$ is characteristic of white noise and the right-hand side of Eq. (2) becomes equal to $2b\delta(\tau)$, where $2b$ is the spectral density. This corresponds to the phase-diffusion model. It should be understood that in Eq. (3), ω is not to be confused with the optical frequency $\omega_L+\omega(t)$ of the laser field. The transform of $\frac{1}{2}\langle E(t)E^*(t+\tau)\rangle$ gives the intensity spectrum of the laser field resulting from the stochastic process $\phi(t)$ on Eq. (1), and can be shown to be[19]

$$P_E(\omega)=\frac{E_0^2}{2}\int_{-\infty}^{\infty}d\tau\exp[-i(\omega-\omega_0)\tau]\times\exp\left[-b|\tau|+b\frac{\exp(-\beta|\tau|)-1}{\beta}\right]\ . \quad (4)$$

In the limit $\beta\gg b$ this gives a Lorentzian spectrum with a FWHM equal to $2b$. If β is also much larger than κ or the Rabi frequency Ω, then the difference between the PDM and BMPDM is negligible. In the limit $b\gg\beta$ the laser spectrum is Gaussian with a FWHM equal to $[8\ln(2)b\beta]^{1/2}$.

The theory of Haslwanter *et al.*[2] treated stationary atoms in a uniform field. Here we extend that work to include the effects of Doppler broadening and spatial variation of the laser intensity within the interaction region. The results of this section, based on the PDM, will be compared to data taken with $\beta=10\kappa$. However, these results can be extended to the BMPDM using the methods of Ref. 3. Our notation is identical with that of Ref. 2.

For a two-level system $\{|0\rangle,|1\rangle\}$ with spontaneous decay rate κ, the elements of the density matrix (solutions of the optical Bloch equations) may be expressed as the atomic coherences $\rho_{10}(t)$ and $\rho_{01}(t)$, and the population difference $w(t)=\rho_{11}(t)-\rho_{00}(t)$, where $\rho_{11}+\rho_{00}=1$. To solve the Bloch equations when the driving field has a stochastically varying phase $\phi(t)$ we make the transformations $\tilde{\rho}_{10}(t)=\rho_{10}(t)\exp[i\phi(t)]$ and $\tilde{\rho}_{01}(t)=\rho_{01}(t)\exp[-i\phi(t)]$. After averaging over the phase fluctuations, the result is a set of differential equations, the solutions of which are the phase-averaged density-matrix elements $\langle\tilde{\rho}_{10}(t)\rangle$, $\langle\tilde{\rho}_{01}(t)\rangle$, and $\langle w(t)\rangle$, where $\langle\ \rangle$ denotes averaging over the phase fluctuations. We are concerned not only with first-order quantities such as the average rate of fluorescence $\langle I(t)\rangle=\kappa\langle\rho_{11}(t)\rangle$, but also with second-order quantities. In the notation of Ref. 2 where $\langle a,b\rangle\equiv\langle ab\rangle-\langle a\rangle\langle b\rangle$, the statistical variance of the fluorescence intensity is given by

$$[\Delta I(t)]^2\equiv\langle I(t),I(t)\rangle=\kappa^2[\langle\rho_{11}(t)^2\rangle-\langle\rho_{11}(t)\rangle^2]\ ,$$

when, as shown in Ref. 3, there are a large number of atoms in the sample (antibunching effects and shot noise are negligible) and the detector area is large.

Now we develop expressions for these quantities when nonstationary atoms are in a spatially nonuniform field. In the notation of this paper, Eq. (2.7) of Ref. 3 may be written

$$\langle I^{(k)}(t)\rangle=\kappa\langle\rho_{11}^{(k)}(t)\rangle$$

as the intensity contribution of the kth atom. If the intensity of the driving field is not constant throughout the interaction volume, the Rabi frequency Ω and, consequently, the elements of the density matrix become functions of position $\mathbf{x}$. Moreover, if the atoms are moving in the interaction region, the density-matrix elements become functions also of velocity $\mathbf{v}=d\mathbf{x}/dt$. Therefore contributions from different atoms become contributions from different positions and velocity groups. Just as above, we move to an appropriate rotating frame with the transformations $\hat{\rho}_{10}(t)=\tilde{\rho}_{10}(t)\exp[-i\mathbf{k}\cdot x(t)]$ and $\hat{\rho}_{01}(t)=\tilde{\rho}_{01}(t)\exp[-i\mathbf{k}\cdot\mathbf{x}(t)]$. In this frame, the averaged density-matrix equations, analogous to Eq. (3.4) of Ref. 2, become

$$\left[\frac{d}{dt}+\begin{bmatrix} z^* & 0 & i\Omega(\mathbf{x})/2 \\ 0 & z & -i\Omega(\mathbf{x})/2 \\ i\Omega(\mathbf{x}) & -i\Omega(\mathbf{x}) & \kappa \end{bmatrix}\right] \times \begin{bmatrix} \langle\hat{\rho}_{10}(\mathbf{x},\mathbf{v})\rangle \\ \langle\hat{\rho}_{01}(\mathbf{x},\mathbf{v})\rangle \\ \langle w(\mathbf{x},\mathbf{v})\rangle \end{bmatrix} = \begin{bmatrix} 0 \\ 0 \\ -\kappa \end{bmatrix}, \quad (5)$$

where $z=b+\kappa/2+i(\Delta+\mathbf{k}\cdot\mathbf{v})$. Here the time dependence of the density-matrix elements has been suppressed for brevity, and the stationary atom detuning Δ is seen to be Doppler shifted to $\Delta+\mathbf{k}\cdot\mathbf{v}$.

For a given laser bandwidth and detuning, Eq. (5) may be solved for $\langle\rho_{11}(\mathbf{x},\mathbf{v})\rangle$. Assuming a large number N of noninteracting atoms, we then integrate over the Maxwellian velocity distribution and the laser-intensity profile in the interaction volume to obtain the Doppler and spatially averaged upper-state population. The corresponding intensity is thus

$$\langle\langle I(t)\rangle\rangle_{x,v}=\kappa\sum_{k}^{N}\langle\rho_{11}^{(k)}(t)\rangle$$

$$=\kappa CN\int d^3x\int d(kv)\langle\rho_{11}(\mathbf{x},\mathbf{v})\rangle \times\exp-\left[\frac{kv}{D}\right]^2, \quad (6)$$

where C is a normalization constant, kv is the scalar $\mathbf{k}\cdot\mathbf{v}$, $D/\sqrt{4\ln 2}$ is the Doppler full width at half maximum, and the outer double angular brackets indicate velocity and spatial averaging. In the remainder of this paper, the subscripts x and v will be omitted unless ambiguity arises.

Second-order quantities, such as the variance, contain cross correlations between different atoms, and we write, in analogy to Eq. (2.8) of Ref. 3 for the contribution from the kth and lth atoms,

$$\langle\langle I(t),I(t)\rangle\rangle=\kappa^2\sum_{\substack{k=1\\k\neq l}}^{N}\sum_{l=1}^{N}\langle\rho_{11}^{(k)}(t),\rho_{11}^{(l)}(t)\rangle$$

$$=C^2N^2\kappa^2\int d^3x\int d^3x'\int d(kv)\int d(kv')\langle\rho_{11}(\mathbf{x},\mathbf{v}),\rho_{11}(\mathbf{x}',\mathbf{v}')\rangle\exp\left[-\left[\frac{kv}{D}\right]^2-\left[\frac{kv'}{D}\right]^2\right]. \quad (7)$$

Again the double angular brackets indicate averaging over the phase and over the spatial and velocity distributions. Using the methods of Refs. 2 and 3 we obtain a matrix equation, analogous to Eq. (3.5) of Ref. 2. This is a 9×9 equation of the form

$$(d/dt+\underline{A})\underline{x}=\underline{y}\ , \quad (8)$$

where

$$\underline{A}=\begin{bmatrix}
z_2^* & 0 & 0 & 0 & \frac{i}{2}\Omega(\mathbf{x}') & \frac{i}{2}\Omega(\mathbf{x}) & 0 & 0 & 0 \\
0 & z_2 & 0 & 0 & 0 & 0 & -\frac{i}{2}\Omega(\mathbf{x}') & -\frac{i}{2}\Omega(\mathbf{x}) & 0 \\
0 & 0 & \kappa-i\mathbf{k}\cdot(\mathbf{v}-\mathbf{v}') & 0 & -\frac{i}{2}\Omega(\mathbf{x}') & 0 & 0 & \frac{i}{2}\Omega(\mathbf{x}) & 0 \\
0 & 0 & 0 & \kappa-i\mathbf{k}\cdot(\mathbf{v}-\mathbf{v}') & 0 & -\frac{i}{2}\Omega(\mathbf{x}) & \frac{i}{2}\Omega(\mathbf{x}') & 0 & 0 \\
i\Omega(\mathbf{x}') & 0 & -i\Omega(\mathbf{x}') & 0 & z_1^* & 0 & 0 & 0 & \frac{i}{2}\Omega(\mathbf{x}) \\
i\Omega(\mathbf{x}) & 0 & 0 & -i\Omega(\mathbf{x}) & 0 & z_1'^* & 0 & 0 & \frac{i}{2}\Omega(\mathbf{x}') \\
0 & -i\Omega(\mathbf{x}') & 0 & i\Omega(\mathbf{x}') & 0 & 0 & z_1 & 0 & -\frac{i}{2}\Omega(\mathbf{x}) \\
0 & -i\Omega(\mathbf{x}) & i\Omega(\mathbf{x}) & 0 & 0 & 0 & 0 & z_1' & -\frac{i}{2}\Omega(\mathbf{x}') \\
0 & 0 & 0 & 0 & i\Omega(\mathbf{x}) & i\Omega(\mathbf{x}') & -i\Omega(\mathbf{x}) & -i\Omega(\mathbf{x}') & 2\kappa
\end{bmatrix},$$

$$\underline{x}=\begin{bmatrix}\langle\hat{\rho}_{10}(\mathbf{x},\mathbf{v}),\hat{\rho}_{10}(\mathbf{x}',\mathbf{v}')\rangle\\ \langle\hat{\rho}_{01}(\mathbf{x},\mathbf{v}),\hat{\rho}_{01}(\mathbf{x}',\mathbf{v}')\rangle\\ \langle\hat{\rho}_{10}(\mathbf{x},\mathbf{v}),\hat{\rho}_{01}(\mathbf{x}',\mathbf{v}')\rangle\\ \langle\hat{\rho}_{10}(\mathbf{x}',\mathbf{v}'),\hat{\rho}_{01}(\mathbf{x},\mathbf{v})\rangle\\ \langle\hat{\rho}_{10}(\mathbf{x},\mathbf{v}),w(\mathbf{x}',\mathbf{v}')\rangle\\ \langle\hat{\rho}_{10}(\mathbf{x}',\mathbf{v}'),w(\mathbf{x},\mathbf{v})\rangle\\ \langle\hat{\rho}_{01}(\mathbf{x},\mathbf{v}),w(\mathbf{x}',\mathbf{v}')\rangle\\ \langle\hat{\rho}_{01}(\mathbf{x}',\mathbf{v}'),w(\mathbf{x},\mathbf{v})\rangle\\ \langle w(\mathbf{x},\mathbf{v}),w(\mathbf{x}',\mathbf{v}')\rangle\end{bmatrix},$$

and

$$\underline{y}=\begin{bmatrix}(2b_1-b_2)\langle\hat{\rho}_{10}(\mathbf{x},\mathbf{v})\rangle\langle\hat{\rho}_{10}(\mathbf{x}',\mathbf{v}')\rangle\\ (2b_1-b_2)\langle\hat{\rho}_{01}(\mathbf{x},\mathbf{v})\rangle\langle\hat{\rho}_{01}(\mathbf{x}',\mathbf{v}')\rangle\\ 2b_1\langle\hat{\rho}_{10}(\mathbf{x},\mathbf{v})\rangle\langle\hat{\rho}_{01}(\mathbf{x}',\mathbf{v}')\rangle\\ 2b_1\langle\hat{\rho}_{10}(\mathbf{x}',\mathbf{v}')\rangle\langle\hat{\rho}_{01}(\mathbf{x},\mathbf{v})\rangle\\ 0\\ 0\\ 0\\ 0\\ 0\end{bmatrix},$$

with

$$z_2=b_2+\kappa+i[2\Delta+\mathbf{k}\cdot(\mathbf{v}+\mathbf{v}')],$$

$$z_1=b_1+3\kappa/2+i(\Delta+\mathbf{k}\cdot\mathbf{v}),$$

$$z_1'=b_1+3\kappa/2+i(\Delta+\mathbf{k}\cdot\mathbf{v}').$$

In these expressions, b_1 and b_2 are defined in Ref. 2, Eq. (2.3), and are related to second- and fourth-order field correlations of the input field, respectively. For the PDM, b_1 is equal to the spectral density b defined in Eq. (2), and $b_2=4b$.

The elements of $\underline{y}$ are obtained from solution of Eq. (5) for the values of $\mathbf{x}$ and $\mathbf{v}$ and again for the values $\mathbf{x}'$ and $\mathbf{v}'$. Then Eq. (8) may be solved for the elements of column matrix $\mathbf{x}$. Note that this 9×9 equation reduces to a 6×6 equation, identical to Ref. 2, Eq. (3.5), when the field has uniform intensity and the atoms are stationary.

The power spectrum of the fluorescence intensity fluctuations has been developed in Ref. 3. In analogy to their Eq. (5.2) we have the power spectrum $P_I(\omega)$, an implicit function of $\mathbf{x}$, $\mathbf{x}'$, $\mathbf{v}$, and $\mathbf{v}'$, given by

$$P_I(\omega)=\frac{\kappa^2\mathrm{Re}}{4}\left[\frac{\langle w(\mathbf{x},\mathbf{v}),w(\mathbf{x}',\mathbf{v}')\rangle-\dfrac{i\Omega(\mathbf{x})\langle\hat{\rho}_{10}(\mathbf{x},\mathbf{v}),w(\mathbf{x}',\mathbf{v}')\rangle}{z^*+i\omega}+\dfrac{i\Omega(\mathbf{x})\langle\hat{\rho}_{01}(\mathbf{x},\mathbf{v}),w(\mathbf{x}',\mathbf{v}')\rangle}{z+i\omega}}{\kappa+i\omega+\dfrac{\Omega(\mathbf{x})^2}{2(z^*+i\omega)}+\dfrac{\Omega(\mathbf{x})^2}{2(z+i\omega)}}\right], \tag{9}$$

where the variances of the density-matrix elements are known from solution of Eq. (8) for a particular detuning. Note $P_I(\omega)=P_I(-\omega)$. This expression is integrated to give the Doppler and spatially averaged power spectrum,

$$\langle P_I(\omega)\rangle_{x,v}=C^2N^2\int d^3x\int d^3x'\int d(kv)\int d(kv')P_I(\omega)\exp\left[-\left[\frac{kv}{D}\right]^2-\left[\frac{kv'}{D}\right]^2\right]. \tag{10}$$

The quantities $\langle(\Delta I)^2\rangle$ and $\langle P_I(\omega)\rangle_{x,v}$ have been calculated assuming a fluorescence detector with infinite bandwidth. The effect of a first-order filter has been treated in Ref. 2, but for detectors with some other frequency response, as in this work, another, but equivalent, method is required. The intensity detected by a detector with arbitrary response function $g(t)$ is

$$I_D(t)=\int_{-\infty}^{t}g(t-t')I(t')dt'. \tag{11}$$

At a given detuning, $\langle P_I(\omega)\rangle_{x,v}$ is calculated and multiplied by the square of the measured frequency response $g(\omega)$ of the detection system, where $g(\omega)$ is the Fourier transform of $g(t)$. The result is a theoretically predicted power spectrum as measured by the real apparatus. This can be integrated over frequency to obtain the variance at that detuning, as in Ref. 3, Eq. (5.1),

$$\langle\langle I_D(t),I_D(t)\rangle\rangle=\int_{-\infty}^{\infty}d\omega|g(\omega)|^2\langle P_I(\omega)\rangle_{x,v}. \tag{12}$$

Figure 1 is a comparison between power spectra calculated with a uniform field intensity (corresponding to a Rabi frequency of 2.5κ) and with a Gaussian intensity profile, both with the same total power. In Fig. 1(a) the spectra are calculated at line center ($\Delta=0$) and in Fig. 1(b) they are calculated at a detuning of $\Delta=3\kappa$, where we have assumed a cylindrically symmetric interaction region. The area under each curve is proportional to the variance. The spectra of the fluctuations produced by a uniform field have maxima near the generalized Rabi frequency $\Omega'=(\Omega^2+\Delta^2)^{1/2}$. However, in the case of a Gaussian beam profile, the power spectrum is an average of spectra produced by different Rabi frequencies, each with its maximum at a different position. When the field

is tuned to line center, the spatial averaging process obliterates the maximum at Ω, but low-frequency components are present in all of the averaged spectra and reinforce, resulting in a maximum at zero frequency. At moderate detunings ($\Delta \approx \Omega$) the low-intensity components of the laser profile contribute less significantly to the fluorescence intensity fluctuations because the overall intensity emanating from these regions is low. Consequently, the spatial averaging is weighted to the high-intensity portions of the laser beam, and the power spectrum shows a local maximum at Ω'.

The above calculations were for zero Doppler width. However, similar results for the spectrum are obtained for Doppler broadening in a spatially uniform beam. Our calculations indicate that the ΔI profile is broadened and the overall fluctuations are reduced for Doppler broadened systems, but the existence of a minimum is relatively insensitive to the Doppler broadening. For example, for the PDM a laser linewidth of $2b = \kappa$ gives a small central minimum in ΔI when there is no Doppler broadening and the field is weak. A Doppler distribution with width equal to at least 20κ is required to wash out the minimum.

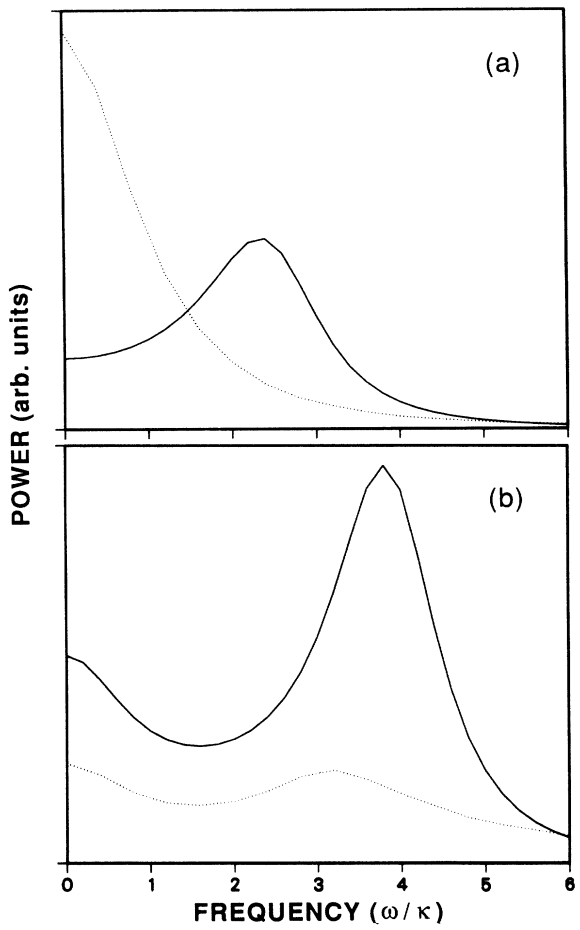

FIG. 1. Theoretically predicted spectra of fluorescence-intensity fluctuations produced by a phase-diffusing field with $b = 0.2\kappa$ for a uniform (solid line) and Gaussian (dotted line) laser-intensity profile, both with the same total power corresponding to $\bar{\Omega} = 2.5\kappa$. In (a) the laser is tuned to line center ($\Delta = 0$) and in (b) $\Delta = 3\kappa$.

III. EXPERIMENT

To produce the phase-diffusing laser field we use the method described by Elliott and Smith[19] in which a Gaussian white-noise source is shaped with an RC filter network to produce noise with a known power spectrum. This noise is then imposed on a frequency-stabilized single-mode ring dye laser with a system of acousto-optic (AOM) and electro-optic (EOM) modulators. For technical reasons an AOM is used for frequency modulation in the range of 0–6 MHz and an EOM is used for phase modulation in the range of 6–200 MHz. The frequency correlation function of the laser modulated in this manner is given by Eq. (2). The bandwidth of the frequency fluctuations β is controlled by the selection of the 3-dB cutoff of the RC filter and the spectral density b is controlled by the power level of the rf noise signal used to drive the AOM and EOM. A direct measurement of the resulting intensity spectrum of the laser field is obtained from a heterodyne signal produced by mixing portions of modulated light and unmodulated light on a fast photodiode. The heterodyne signal, composed of the difference frequencies of the two beams, is resolved with an rf spectrum analyzer. The modulation system has been designed such that measurements of the spectrum of the laser field agree to Eq. (4) to within 1 dB ($\pm 12\%$ in amplitude).

A schematic of our experiment is shown in Fig. 2. The setup is very similar to one previously described for an experiment on the Autler-Townes effect.[10] The two-level system was prepared in a beam of atomic sodium. The sodium $3S_{1/2} \rightarrow 3P_{3/2}$ transition has a natural linewidth of 10 MHz and is convenient for our noise modulation system, which can produce laser linewidths in the range of 1–20 MHz. This linewidth also ensures that the residual Doppler broadening of approximately 7.5 MHz did not dominate over the natural linewidth.

To provide a two-state system and control the laser scan, a portion of the laser was split off prior to noise modulation and modulated with an EOM to produce variable frequency-modulated (FM) sidebands. This beam was circularly polarized and directed into the atomic beam ahead of the interaction region and the upper sideband was tuned into resonance with the atoms thereby optically pumping the atoms into the $F = 2$, $m_f = 2$ hyperfine state. In addition, the FM sidebands were frequency modulated (dithered) at a much lower frequency of 1 kHz. The fluorescence from the pumping region was detected and analyzed at the dither frequency with a lock-in amplifier. The lock-in amplifier generated an error signal which, when input to the scan control of the ring dye laser, regulated the laser carrier frequency ω_L such that the upper sideband of the optical pumping beam remained locked on resonance. The AOM in the noise modulation system produces a net positive 400-MHz offset of the input laser carrier frequency, so when the upper FM sideband of the optical pumping beam was tuned to $\omega_L + 400$ Mz the noise-modulated laser beam was at zero detuning (small deviations from zero detun-

ing exist due to skewness of the two beams in the interaction region). The scanning of the noise-modulated laser was achieved by scanning the frequency of the FM signal to the EOM [Fig. 2(b)]. A heterodyne signal, obtained from portions of the noise-modulated beam and optical pumping beam, provides a measurement of the detuning of the noise-modulated laser. The noise-modulated laser was also circularly polarized to couple the prepared ground state to only the $F=3$, $m_f=3$ hyperfine level of the $3P_{3/2}$ upper state, thus providing a two-level system.[20] The Earth's magnetic field in the interaction region was nulled with a three-dimensional arrangement of Helmholtz coils to less than 10 mG, and a magnetic field of 500 mG applied along the direction of propagation of the laser beams. The 500-mG field maintains the orientation of the ground state by breaking the degeneracy of the magnetic sublevels, thus reducing mixing by stray fields.

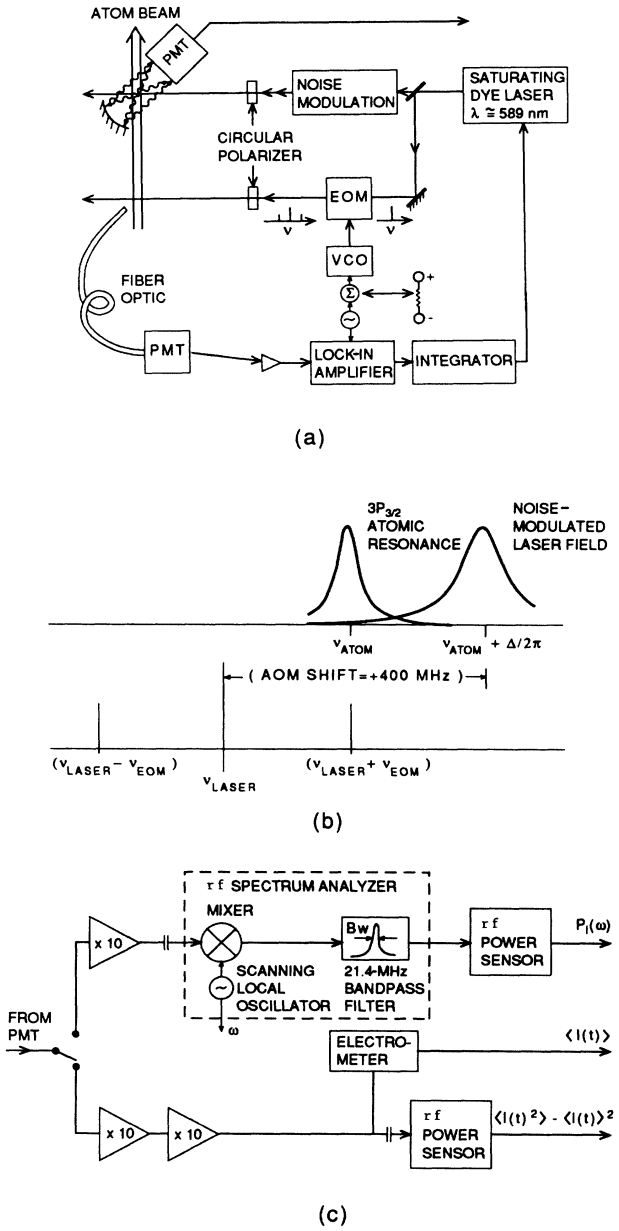

FIG. 2. Schematic diagram of the experiment: (a) Details of the apparatus. The upper sideband from the optical pumping beam is locked on resonance by feeding a signal derived from the pumping fluorescence back to the dye laser. The dye-laser frequency at $\nu_L=\nu_{\text{atom}}-\nu_{\text{EOM}}$ is offset by an acousto-optic modulator in the noise-modulation system. The noise-modulated laser frequency at $\nu_{\text{noise}}=\nu_{\text{atom}}-\nu_{\text{EOM}}+400$ MHz is scanned by scanning ν_{EOM}. (b) Illustration of the frequencies of the optical pumping and the noise-modulated lasers. The detuning of the noise-modulated laser is $\Delta/2\pi=400$ MHz $-\nu_{\text{EOM}}$. (c) The detection electronics.

Predictions from Ref. 2 give the ratio of the rms intensity fluctuations $\Delta I\equiv[(\Delta I)^2]^{1/2}$ to the average intensity $\langle I\rangle$ to be about 30–40 %. The bandwidth of the fluctuations is given approximately by the larger of b, κ, or Ω', as can be seen from the arguments given in Sec. I. The shot noise due to the photodetection process could have dominated the intensity fluctuations if appropriate care was not taken. The shot-noise contribution to the rms current at the detector output adds in quadrature to that due to the rms intensity fluctuations, and can be calculated from the formula $\Delta i=\sqrt{2eibw}$, where i is the average current at the cathode of the detector, bw is the detection bandwidth, and e is the charge of an electron. The current at the cathode is given by $i=e\eta I_p$, where η is the quantum efficiency of the detector (equal to 0.08) and I_p is the photon current. The shot noise is reduced relative to the intensity fluctuations as the detection bandwidth is reduced, until the detection bandwidth equals the bandwidth of the intensity fluctuations. At this point, further reduction of the detection bandwidth reduces both the power of the shot noise and the intensity fluctuations equivalently, and there is no further enhancement of the rms intensity fluctuations over the shot noise. For this experiment we worked with Rabi frequencies up to 3κ or 30 MHz, requiring a detection bandwidth of about 50 MHz. The requirement that $\Delta i/i$ be much smaller than 30% (so that the shot noise is smaller than the intensity fluctuations) corresponds to photon currents at least on the order of 10^{12} photons sec^{-1}. To achieve this, we collected approximately 50% of the solid angle by placing an RCA C7164R photomultiplier tube (PMT) with a 4.3-cm end-on photocathode 1.5 cm from the interaction region and reflecting the radiation emitted in the opposite direction back into the PMT with a 1.3-cm focal-length mirror. The measured noise level was usually about twice the anticipated shot-noise level, with the difference attributed to PMT gain noise. Fluctuations in the number of atoms in the interaction region contribute to the noise level $\Delta I/\langle I\rangle$ as $N^{-1/2}$, but were negligible because N was typically about 5×10^5. Amplitude fluctuations on the dye laser were -82 dB $\text{Hz}^{-1/2}$ (ac-dc ratio of 7.9×10^{-5} $\text{Hz}^{-1/2}$) below the dc level and had a 3-dB bandwidth of 100 kHz that is at the low end of the frequency range of interest for this experiment, and for these reasons were negligible.

Due to the high photon current, eight dynodes were used in the PMT (from a total of ten), limiting the gain to the range of 10^3–10^4. The ninth dynode was used as the signal anode and terminated at 50 Ω to reduce transmis-

sion line effects. Depending on the light levels into the PMT the chain current was operated in a range from 1.6 to 2.0 mA by adjusting the supply voltage, and the maximum average anode current was 0.1 mA (at zero detuning with the phase noise off). Real-time oscilloscope traces of the PMT output demonstrated that when the laser was at zero detuning with the phase noise on, the intensity flucutations were predominantly negative, so 0.1 mA provided an approximate upper bound to the anode current. Nevertheless, the linearity was carefully checked against a photodiode and deviations were 3% at 0.3 mA and less than 1% at 0.1-mA anode current, despite the rather high ratio of anode to chain current.

The detector and amplifying electronics were carefully characterized. Stray capacitances in the PMT and differing input and output impedances in the amplifiers for the ac and dc components of the signal give rise to differences in the ac and dc gains. An overall scale factor, which accounts for these differences in the data analysis, was determined with a calibrated light source produced by amplitude modulating a laser beam at 4 MHz. This light source was used to illuminate the PMT and a fast photodiode, and the output wave forms were compared on an oscilloscope. The ratio of the rms voltage to dc voltage when measured by the PMT was a factor of 2.25 ± 0.10 lower than when measured with the photodiode. The frequency response $g(\omega)$ of the detector and electronics was measured by illuminating the PMT with a sine-wave-modulated light source, produced by heterodyning two laser beams, and recording the amplitude of the signal at the frequency as one laser was scanned. These measurements indicated a 3-dB point of 45 MHz with a roll off of approximately 16 dB octave.$^{-1}$

In Sec. II it was shown that the spatial wings of a Gaussian TEM_{00} mode laser beam had the effect of washing out the side peaks at the Rabi frequency in $P_I(\omega)$. To reduce this effect, it was necessary to remove the spatial wings of the Gaussian beam. It was not possible to collect light only from the central section of the interaction region using optical imaging methods. The noise-modulated beam was first spatially filtered to produce the TEM_{00} mode. Then an aperture was placed at the output of the spatial filter and adjusted to remove the wings. This image was then brought into focus at the interaction region with a system of lenses, thus nearly eliminating the diffusion effects of the aperture. Pinhole scans of the resulting beam indicated a beam 1.7 mm in diameter with a near-Gaussian central section extending out to approximately 70% of the FWHM. The beam also contained narrow wings (approximately 0.1 mm) outside the Gaussian portion due to residual diffraction.

We conclude this section with a discussion of the methods by which the variance and spectrum of the intensity fluctuations are obtained from the PMT signal [Fig. 2(c)]. To measure the variance of the fluorescence intensity the signal from the PMT was amplified by a factor of 100 with two 50-Ω input broadband amplifiers. As the noise-modulated laser was scanned across the transition the dc component of the signal was determined with an electrometer and the rf power was measured with a power sensor consisting of a capacitively blocked 50-Ω resistor thermally coupled to a monolithic silicon thermocouple. The power sensor measures the true mean of the square of the ac component. Power levels were typically in the 0–30-μW range and dc voltage levels in the range of 0–0.25 V. The rf power and the dc voltage are proportional to the variance $(\Delta I)^2$ and the time average $\langle I(t)\rangle$ of the intensity, respectively. These quantities were then logged by a computer as functions of the laser detuning. The ac power in the signal is dissipated across 50 Ω in the power sensor and is converted to a rms voltage using the formula $V_{\rm rms}=2.25\sqrt{50P'}$, where P' is the measured power after correction for shot noise. The scale factor 2.25 has been applied to $V_{\rm rms}$ as discussed above. The rms voltage, which is proportional to ΔI, is thus put on the same scale as the dc voltage level, which is proportional to $\langle I(t)\rangle$. Low-intensity scans required a small correction for the shot noise since the light levels into the detector were lower. This correction makes use of the fact that the shot-noise power scales linearly with the dc voltage and thus $\langle I(t)\rangle$. Since the power of the shot noise is additive,[3] the corrected power was calculated as $P'=P-\alpha\langle I(t)\rangle$, where α is a scale factor determined from scans with the noise modulation off, and P is the actual measured power level. For the low-power scans $\alpha\langle I(t)\rangle\approx0.1P'$ at line center, which gives a 5% correction for ΔI. The shot-noise corrections were negligible for high-intensity scans.

Spectra of the intensity fluctuations were taken with the laser at a fixed detuning and one broadband amplifier removed. A commercial spectrum analyzer was used as a tunable bandpass filter with the bandwidth typically set at 100 kHz and the center frequency tuned from 0 to 100 MHz. In the spectrum analyzer, the signal is mixed with the output of a tunable local oscillator and the resulting signal is passed through a 21.4-MHz bandpass filter. The power in the 21.4-MHz signal, proportional to the spectrum of the intensity fluctuations $P_I(\omega)$, is measured with the power sensor. The statistics of the intensity fluctuations are not known and could conceivably be a function of the laser detuning and intensity if the laser is saturating, so it was necessary to measure the true power in the 21.4-MHz signal. Our spectrum analyzer is equipped with an envelope detector that measures the average of the absolute amplitude, not the squared amplitude, which can result in systematic errors.

IV. RESULTS AND DISCUSSION

A. Variance of the intensity fluctuations

In Fig. 3 we present data collected with $\beta/2\pi=100$ MHz and values for the spectral density b, which give laser linewidths of approximately 4, 10, and 15 MHz, and spatially averaged Rabi frequencies of approximately 2, 10, and 25 MHz. Measurements of $\Delta I\equiv[(\Delta I)^2]^{1/2}$ and $\langle I(t)\rangle$ are shown in the lower double-peaked curve and upper curve, respectively. The theoretical calculations are shown as circles or squares plotted over the data. The theoretical calculations of Fig. 3 are based on the methods of Sec. II for $\beta\rightarrow\infty$. In these data $\beta/2\pi=100$ MHz, which is a good approximation to this case.

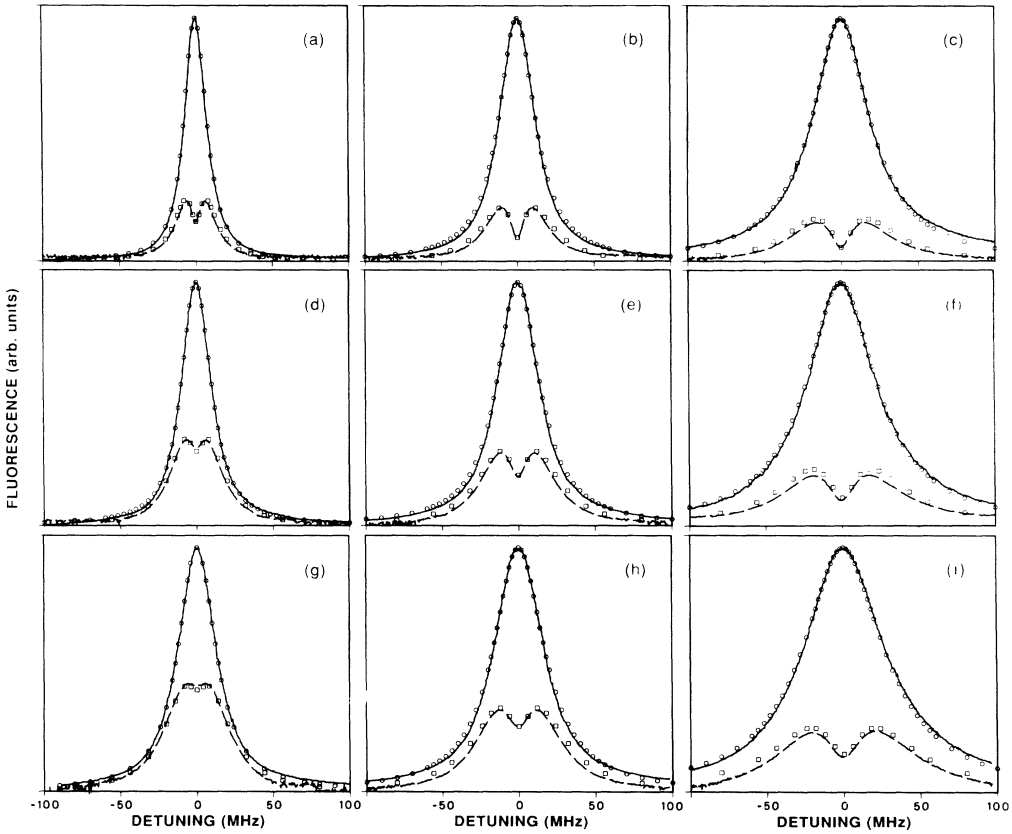

FIG. 3. Experimental fluorescence intensity $\langle I(t)\rangle$ (solid line), rms fluorescence-intensity fluctuations ΔI (dash-dotted line), and theoretical predictions (circles and squares, respectively) vs detuning of the phase diffusing laser for $\beta/2\pi = 100$ MHz. The values of of $b/2\pi$ and the spatially averaged Rabi frequency $\bar{\Omega}/2\pi$ (MHz) are, respectively, (a) 2.0, <2; (b) 2.0, 12 ; (c) 2.0, 25; (d) 5.0, <2; (e) 5.0, 11; (f) 5.0, 25; (g) 8.3, <2; (h) 7.5, 12; and (i) 7.5, 25. The plots are organized such that the Rabi frequency is approximately constant within a column and the laser FWHM equal to $2b$ is constant within a row.

A number of parameters were necessary for the calculations shown in Fig. 3. The value for β is known from the shaping filters in the noise generation system. The value of b is obtained from fits of numerical solutions of Eq. (4) to heterodyne measurements of the laser spectrum. The value of residual Doppler broadening was obtained from low-intensity scans with the noise off and ranged from 7.5 to 8.0 MHz (giving 14 MHz total linewidth for sodium).

The calculations assumed an intensity distribution (to be discussed in Sec. IV B) for the spatial averaging of Eqs. (6), (7), and (10). Using this intensity distribution, numerical solutions of Eq. (6) were compared to actual measurements of $\langle I(t)\rangle$ as a function of laser detuning. The value of the total laser power which gave the same degree of saturation broadening for the calculated and measured $\langle I(t)\rangle$ was then used for the calculations of the variance and spectrum [Eqs. (7) and (10)]. The quoted Rabi frequencies in the figures are based on the equivalent Rabi frequency necessary to give the same amount of saturation broadening, fitted in the region of the half-width, assuming a uniform laser beam and thus represent a spatially averaged value (denoted by $\bar{\Omega}$). The laser power and Rabi frequency determined this way were typically within 5% of the values obtained from a direct measurement of the laser power with a calibrated photodiode.

Corrections to the data and calculations of Fig. 3 were made as follows. The data for $\bar{\Omega}/2\pi < 2$ MHz and $\bar{\Omega}/2\pi \approx 10$ MHz were corrected for the shot noise as discussed in Sec. III. As mentioned previously, this was not necessary for $\bar{\Omega}/2\pi \approx 25$ MHz. For $\bar{\Omega}/2\pi < 2$ MHz, the calculations included the effects of Doppler broadening, but for weak fields the ratio $\Delta I/\langle I\rangle$ is independent of Ω so a correction for laser-intensity variation across the interaction region was not necessary. For scans with $\bar{\Omega}/2\pi \approx 10$ MHz, the calculations were corrected for both Doppler and spatial intensity variation. At high intensity ($\bar{\Omega}/2\pi = 25$ MHz) the Doppler broadening was small compared to the saturation broadened linewidth, so corrections were made only for spatial-intensity variation. Furthermore, a correction for the detector response has been made for all of the theoretical plots in Fig. 3 according to Eq. (12). To give an idea of the magnitude of the corrections, Fig. 4 shows the corrections added sequentially for a ΔI profile calculated with the parameters of Fig. 3(e). We emphasize that, with the exception of the shot-noise correction, all of the corrections are made to the theoretical calculations so that the calculations take actual experimental conditions into account.

As can be seen in Fig. 3, the agreement between theory and experiment for the low-power scans is quite good with discrepancies on the order of only a few percent. As

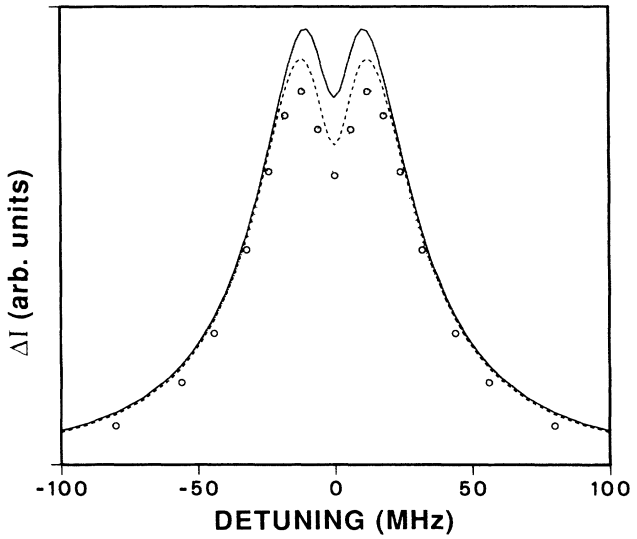

FIG. 4. Theoretically predicted rms fluorescence-intensity fluctuations ΔI for $b/2\pi=5$ MHz and $\bar{\Omega}/2\pi=11$ MHz from the theory of Haslwanter *et al.* (Ref. 2) (solid line), from the theory presented in this work with 8-MHz Doppler broadening (dashed line), with 8-MHz Doppler broadening, and truncated Gaussian laser-intensity profile as described in the text (dotted line), and the former with detector response treated as described in the text (circles).

the power level is increased the agreement is less good (discrepancies of up to 15%), most likely to a lack of knowledge of the precise intensity distribution across the interaction region, a point that will be discussed in more detail.

A number of trends are evident in Fig. 3. Within a column with uniform $\bar{\Omega}$ the extent of the central dip in ΔI is reduced as the bandwidth of the laser spectrum is increased (the FWHM equals $2b$). The two peaks of ΔI are no longer resolved in the low-power scans when the FWHM of the laser becomes comparable to the natural linewidth κ. For a given value of b, the extent of the dip increases and the overall magnitude of the fluctuations is reduced as the power level of the laser is increased. For a detector of infinite bandwidth, Ref. 3 predicts a much higher noise ratio $\Delta I/\langle I\rangle$ in the wings of the ΔI profile than is observed in Fig. 3. The bandwidth of the intensity fluctuations increases with the detuning due to contributions to $P_I(\omega)$ at Ω'. Consequently, as the laser is detuned more of the power in the spectrum of the intensity fluctuations is shifted beyond the bandwidth of the detector resulting in a reduction in the wings of the profile of ΔI (see Fig. 4). The effect of finite β is qualitatively similar to that of a finite detector response and becomes appreciable if Ω' approaches the value of β. For $\beta/2\pi=100$ MHz and these intensity levels, finite-β effects are quite small except in the region of the far wings.

B. Spectra of the intensity fluctuations

Spectra of the intensity fluctuations for the parameters of Figs. 3(a) and 3(c) are shown in Figs. 5(a) and 5(b), respectively. The calculated spectra, with the same corrections as discussed for Fig. 3, are shown in Figs. 5(c) and 5(d). The data at low frequencies are obscured by local oscillator effects of the spectrum analyzer and are not shown. In Fig. 5(a), a discontinuity in the spectra at 6 MHz is due to imperfect matching of the individual shaping filters for the AOM and EOM, which shape the spectrum of the frequency fluctuations of the input field to Eq. (3). In addition, the spectra of Fig. 5(b) with $\bar{\Omega}/2\pi=25$ MHz contain discontinuities at 15, 25, and 35 MHz which are due to spurious resonances of the $LiTaO_3$ crystal of the EOM. These artifacts are not apparent in the variance of the fluorescence or in the heterodyne measurements of the laser spectrum. Clearly, the spectrum of the intensity fluctuations is very sensitive to details in the spectrum of the laser-frequency fluctuations. Since the variance is proportional to the integral of the $P_I(\omega)$, these artifacts are effectively averaged out in the data plots of variance versus detuning.

Despite the discrepancies mentioned above, the data in Fig. 5 are qualitatively in agreement with the calculations. In Fig. 5(a), for $\bar{\Omega}/2\pi<2$ MHz (below saturation) and $\Delta=0$, it can be seen that the fluctuations roll off at frequencies of approximately $\kappa/2\pi$. The spectra become broader as the laser is detuned from resonance, as predicted in Ref. 3, due to the excitation of transients at frequencies given by the laser detuning. For laser detunings of $\Delta/2\pi\gtrsim 30$ MHz and $\Omega/2\pi<2$ MHz, Ref. 3 predicts a peak located at Δ that is resolved from the central peak, but the overall magnitude of the fluctuations is much too small for it to be observed in this experiment. When the laser power is increased, as in Fig. 5(b) where $\bar{\Omega}/2\pi\approx 25$ MHz, the features of the spectra are broadened considerably, in this case due to excitation of transients which contribute to $P_I(\omega)$ at the generalized Rabi frequency Ω'. For the curve with $\Delta/2\pi=30$ MHz, the peak at the generalized Rabi frequency is clearly evident. The arrows in Fig. 5(b) locate the value of Ω' and thus the positions at which the peaks are expected to occur. The peak at Ω', in the spectra for $\Delta/2\pi=15$ MHz, is just beginning to become resolved.

In Fig. 5, the quantitative agreement between theory and experiment for these spectra is not as close as for the variances. At low power this is due primarily to the effects of the 6-MHz matching point and EOM resonances. At high power, in addition to these artifacts, effects of a finite $\beta/2\pi$ of 100 MHz lead to a further reduction of the spectra at higher frequencies. A calculation with $\beta/2\pi=100$ MHz gives a 10% reduction at 40 MHz when compared to $\beta=\infty$. However, as in the variances, we feel the largest uncertainty is due to intensity distribution across the interaction region. Each spatial value of the intensity, hence the Rabi frequency, contributes to the integration of $\langle\rho_{11}(\mathbf{x},\mathbf{v}),\rho_{11}(\mathbf{x}',\mathbf{v}')\rangle$ over $\mathbf{x}$ and $\mathbf{x}'$ given by Eq. (7). It should be noted that the observed zero detuning spectrum shown in Fig. 5(b) lies somewhere in between that for the Gaussian and uniform intensity profiles shown in Fig. 1(a), indicating a partial removal of the spatial wings of the Gaussian laser distribution by the aperture method described in Sec. III.

We found that the calculations were very sensitive to details of the spatial-intensity distribution of the laser

We found that the calculations were very sensitive to details of the spatial-intensity distribution of the laser beam, particularly in the region of the wings of the distribution. For the calculations, a cylindrically symmetric distribution was used with a central Gaussian profile, truncated at approximately 70% of the FWHM, and with narrow wings continuing thereafter, adopted to fit (within experimental resolution) the measured distribution. This geometry is based on the imaging method discussed in Sec. III. Numerical calculations of Eq. (10), neglecting the contribution from these wings, predict larger Rabi peaks in the spectrum than are observed, suggesting the actual intensity distribution had a larger spread of Rabi frequencies. Shaping of the wings of the distribution, which was within experimental resolution of pinhole scans, resulted in the predicted spectrum for $\Delta=0$, shown in Fig. 5(d), which can be compared to the measured $\Delta=0$ spectrum in Fig. 5(b). This intensity distribution was then adopted for all calculations (spectra and variances) with $\bar{\Omega}$ above saturation. The slight irregularities in the calculated spectra in Fig. 5(d) reflect irregularities in the adopted intensity distribution. This distribution is not necessarily unique, and slightly different distributions gave a better fit of the calculated spectrum to the observed spectrum at other detunings. The true distribution was typically somewhat asymmetric (due to errors in the centering of the apparatus) with slight residual diffraction effects and defects due to optics. Furthermore, the interaction region was in the shape of two intersecting cylinders. All of these factors affect the actual spectrum. It was certainly clear that the data could be fit with a suitable intensity distribution. However, considering the difficulty involved in the measurement of the actual distribution to the required level of precision, the complexity of handling the calculations with a more complicated geometry, and the small gain in physical understanding, we did not pursue this task any further.

An interesting feature of all of the spectra we measured at zero detuning is the lack of discontinuities. Although a quantitative explanation of this effect is lacking, simple models that consider single-tone and double-tone phase modulation provide some physical insight. Single-tone modulation with a small modulation index δ produces a component at ω_1 in the input field frequency spectrum $P_\omega(\omega)$ and also produces a component at ω_1 in the spectrum of fluorescence intensity fluctuations $P_I(\omega)$. The intensity spectrum of the laser field $P_E(\omega)=|E(\omega)|^2$ will also have sidebands at $\omega_0\pm\omega_1$, so at detunings of $\Delta=\pm\omega_1$ one of the sidebands comes into resonance with the atomic transition, which enhances the contribution to $P_I(\omega)$ at

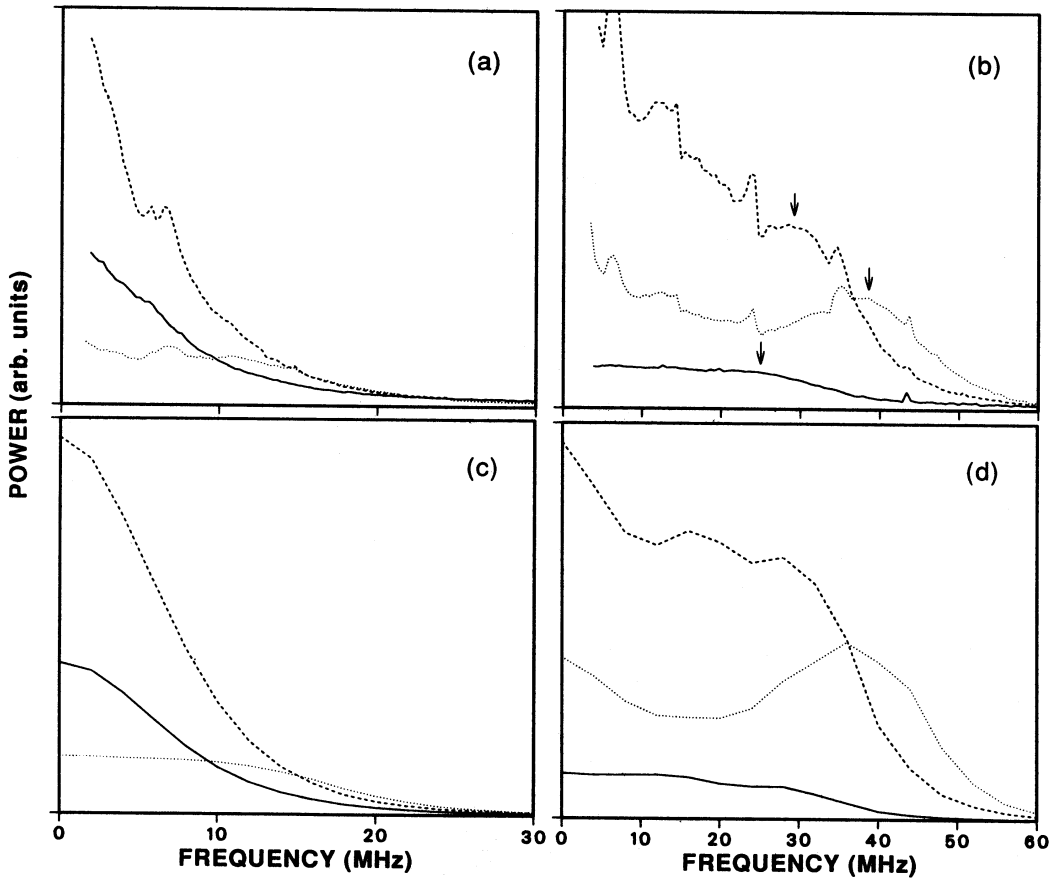

FIG. 5. Spectra of the fluorescence intensity fluctuations $P_I(\omega)$ with $\beta/2\pi=100$ MHz obtained (a) and (b) experimentally, and (c) and (d) theoretically. In (a) and (c) $b/2\pi=2.09$ MHz, and $\bar{\Omega}/2\pi<2$ MHz at detunings of $\Delta/2\pi=0$ (solid line), 5 MHz (dashed line), and 15 MHz (dotted line). In (b) and (d) $b/2\pi=2.0$ MHz and $\bar{\Omega}/2\pi\approx25$ MHz at detunings of $\Delta/2\pi=0$ (solid line), 15 MHz (dashed line), and 30 MHz (dotted line). Note the change of scales.

ω_1. This contribution is proportional to the power in the sideband (i.e., δ^2). The two sidebands of the laser field $E(\omega)$ have equal but opposite amplitudes (opposite phase), which results in a cancellation at zero detuning. Thus the contribution at $P_I(\omega=\omega_1)$, which is large for $\Delta\approx\omega_1$, becomes vanishingly small at $\Delta=0$. It can also be shown, for double-tone modulation at ω_1 and ω_2 that $P_I(\omega)$ will contain a small contribution at $\omega_1-\omega_2$ that does not vanish even at zero detuning. This term, proportional to the product of the power in the sidebands of the two frequencies, is of order δ^4 and except at $\Delta=0$ is normally small compared to the single-tone effects (of order δ^2) at ω_1 and ω_2. The mixing of frequency components can be important when $P_\omega(\omega)$ consists of a resonance at ω_1 in the presence of broadband phase modulation. When the laser is at zero detuning ω_1 will mix with all of the other frequencies, producing small contributions to $P_I(\omega)$ over a continuous frequency range, and spread the effect of the resonance across the entire spectrum. This is similar to a heterodyne process and is quite dramatic if the noise signal to the AOM is turned off, which produces a gap in $P_\omega(\omega)$ from 0 to 6 MHz. Bands of frequency components in $P_\omega(\omega)$ above 6 MHz mix to produce bands of components in $P_I(\omega)$ at lower frequencies, largely filling in $P_I(\omega)$ from 0 to 6 MHz. This effect is only appreciable when the laser is at zero detuning, since only then do the single-tone modulation effects cancel. When the laser is detuned, the single-tone effects take over and a gap quickly develops between 0 and 6 MHz.

C. Finite correlation time of the phase fluctuations

Spectra of the intensity fluctuations for $\bar{\Omega}/2\pi\approx25$ MHz; $\Delta/2\pi=30$ MHz; $\beta/2\pi=100$, 30, and 10 MHz; and $b/2\pi=2.0$, 2.1, and 2.5, respectively, are shown in Fig. 6. The values of b are chosen to maintain the measured laser FWHM between 4 and 5 MHz [since the spectral width for Eq. (4) depends on both b and β]. The area under the data plots is proportional to the variance at $\Delta/2\pi=30$ MHz (Fig. 7). Figure 6(b) shows the calculated spectra for the same parameters, using the methods of Ref. 3 for finite β, but with no corrections for spatial-intensity distribution or Doppler broadening. The overall scale of Fig. 6(b) is reduced relative to Fig. 6(a). Again, the effects of the spatial-intensity distribution are clearly evident in the data.

The general effect of finite β is a reduction of the spectra at frequencies greater than $\beta/2\pi$. This continues as β is reduced below κ, and for $\beta/2\pi=1$ MHz (shown in the inset with $b/2\pi=4.5$ MHz) the spectrum is devoid of structure resulting from the dynamics of the atom. At $\beta/2\pi=10$ MHz only a trace of the peak at Ω' is visible.

Profiles of ΔI, for the same parameters as in Fig. 6, are shown in Fig. 7. There is a general trend to reduce the magnitude of the fluctuations as β is decreased. This effect is more pronounced at high power, as in Fig. 6, than at low power. At high power the PDM ($\beta\rightarrow\infty$) predicts an increase in the bandwidth (approximately equal to Ω') of the fluctuations as the laser power is increased. If β is comparable to Ω', then a reduction of the magnitude of the fluctuations results (as compared to the case of $\beta\rightarrow\infty$). As previously discussed, since Ω' increases with detuning, a finite β will also have more effect in the wings of the ΔI profile.

D. Correlated amplitude and phase fluctuations

In Fig. 7(a), for $\beta/2\pi=1$ MHz, it can be seen that the profile of ΔI is slightly asymmetric. At this value for β, the AOM is responsible for most of the modulation of the laser field. The AOM is also more prone to induce spurious amplitude modulation since the transmission of the AOM is dependent on the frequency of the input rf signal. If the center frequency of the rf signal is not matched to the center frequency of the AOM response, then the AOM will induce correlated amplitude fluctuations. The laser beam is also reflected back through the AOM in a double-pass configuration to cancel angular displacement of the beam when the rf signal is modulat-

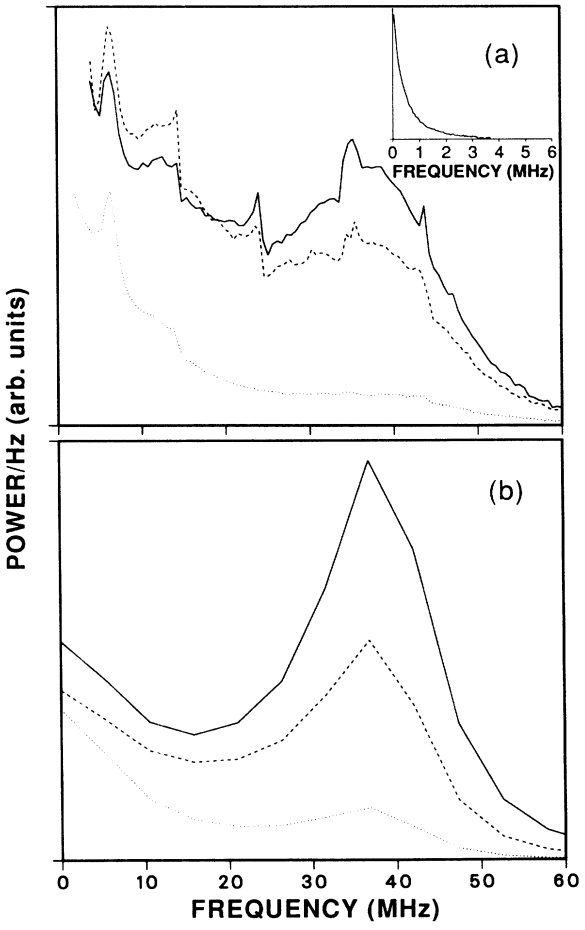

FIG. 6. Spectra of fluorescence intensity fluctuations $P_I(\omega)$ obtained (a) experimentally and (b) theoretically for $\bar{\Omega}/2\pi\approx25$ MHz and $\Delta/2\pi=30$ MHz. The laser FWHM is constant at approximately 4.5 MHz and the statistical parameters of the field are $\beta/2\pi=100$ MHz and $b/2\pi=2.0$ MHz (solid lines), $\beta/2\pi=30$ MHz and $b/2\pi=2.1$ MHz (dashed lines), $\beta/2\pi=10$ MHz and $b/2\pi=2.5$ MHz (dotted lines), and $\beta/2\pi=1.0$ MHz and $b/2\pi=4.5$ MHz (inset). The spectra are normalized to the same fluorescence intensity at line center.

ed. This cancellation requires careful alignment, and small residual errors lead to residual angular displacements of the beam which look like correlated amplitude and frequency fluctuations in the frame of atoms at the edge of the interaction region. The effect of correlations in amplitude and frequency is to produce an asymmetric profile of the intensity fluctuations. This results from the fact that an increase in the amplitude always produces an increase in the fluorescence intensity, whereas for frequency fluctuations this depends on the sign of the laser detuning. Thus the effects of correlated amplitude and frequency fluctuations reinforce on one side of the transition, but tend to cancel on the other.

Figure 8 is a series of data plots that show this effect more clearly for $\beta/2\pi=100$ MHz, $b/2\pi=2$ MHz, and $\bar{\Omega}/2\pi<2$ MHz. The correlated amplitude fluctuations were produced by rotating the polarization of the laser field in the EOM relative to the applied to the rf field.

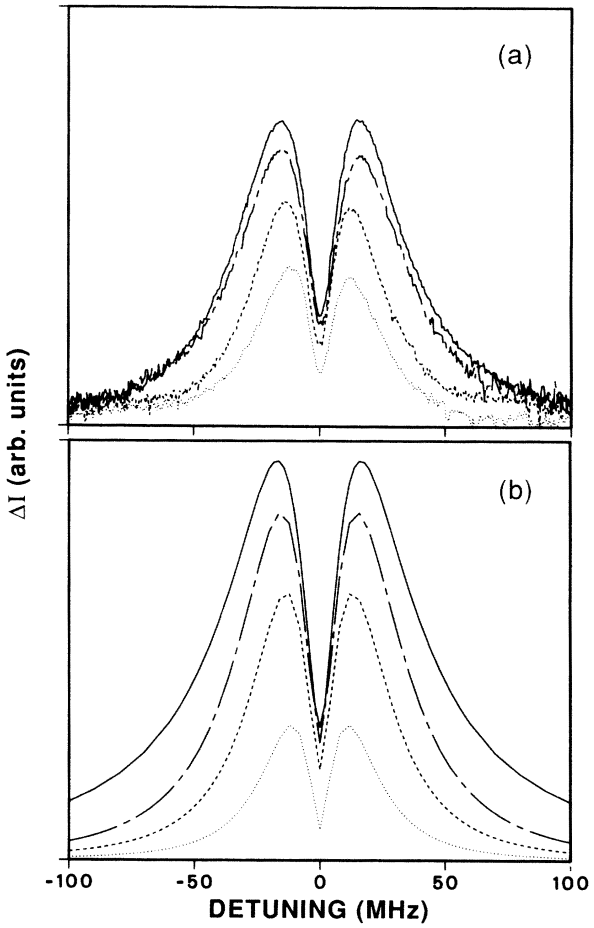

FIG. 7. Relative rms fluorescence intensity fluctuations ΔI obtained (a) experimentally and (b) theoretically for $\bar{\Omega}/2\pi\approx25$ MHz with constant laser FWHM approximately equal to 4.5 MHz. The statistical parameters of the field are $\beta/2\pi=100$ MHz and $b/2\pi=2.0$ MHz (solid lines), $\beta/2\pi=30$ MHz and $b/2\pi=2.1$ MHz (short-dashed–long-dashed lines), $\beta/2\pi=10$ MHz and $b/2\pi=2.5$ MHz (dashed lines), and $\beta/2\pi=1.0$ MHz and $b/2\pi=4.5$ MHz (dotted line). The plots have been normalized to the same fluorescence intensity at line center.

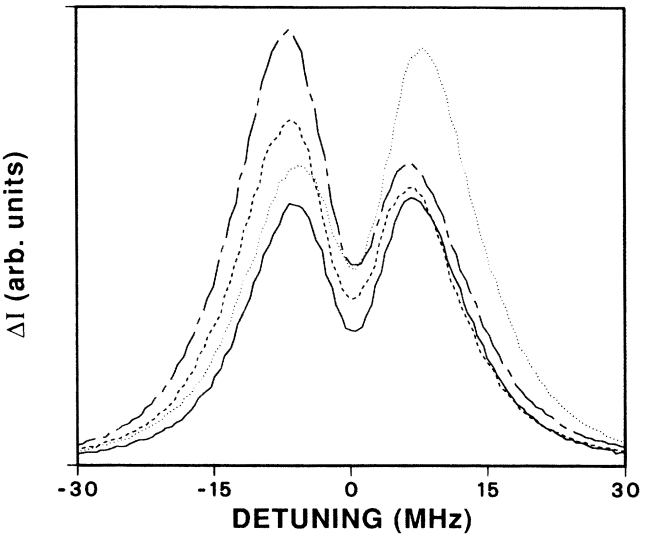

FIG. 8. Measured relative rms fluorescence intensity fluctuations ΔI with and without correlated amplitude fluctuations for $b/2\pi=2.0$ MHz, $\beta/2\pi=100$ MHz, and $\bar{\Omega}/2\pi<2$ MHz. The plots are for no amplitude fluctuations (solid line) and ratios of rms to average intensity of the input beam of $\Delta I_0/I_0\approx0.04$ (short-dashed–long-dashed line), 0.02 (dashed line), and 0.04 with the relative phases of the amplitude and phase fluctuations reversed (dotted line).

The phase of the field component along the direction of the applied rf field is modulated relative to the orthogonal component resulting in polarization modulation. This becomes amplitude modulation after passing through an output polarizer. The amplitude fluctuations were correlated to the frequency (phase) fluctuations from 6 to 200 MHz. The two curves with the largest asymmetry (dotted and dashed lines) had a ratio of rms intensity to dc intensity of $\Delta I_0/I_0\approx0.04$ on the input beam, where I_0 is the intensity of the input beam (and, of course, $\Delta I_0=0$ for pure phase modulation). In the dashed curve $\Delta I_0/I_0$ was about a factor of 2 less and the amplitude fluctuations for the solid line were negligible for the symmetric curve. The curve with the reversed asymmetry was obtained with the polarizer angle reflected about the axis of the applied rf field, thus reversing the relative phase of the amplitude and frequency fluctuations. Calculations were carried out in Ref. 3 for the rotating Vander-Pol oscillator with coupled amplitude and phase noise. These calculations are consistent with our observations. This asymmetry could provide a useful measure of amplitude and phase correlations and diode lasers, and such investigations are now underway in other laboratories.[21]

V. CONCLUSIONS

In conclusion, we have measured the variance of fluorescence intensity and the spectrum of the intensity fluctuations from a two-level system driven with a phase-diffusing laser field. In the low-field limit, our results agree with the predictions of Haslwanter *et al.*[2] to within

a level of a few percent provided Doppler effects are considered. At higher fields, discrepancies become larger, presumably due to the effects of variations in the spatial laser-intensity distribution across the interaction region. At low laser intensity the spectrum of the intensity fluctuations at zero laser detuning consists of a peak at $\omega=0$ with a width given by κ. The bandwidth of the low-intensity spectrum increases with the laser detuning due to the appearance of (unresolved) peaks at the laser detuning. At high laser intensity the overall bandwidth of the spectrum increases, and the spectrum contains a peak at the generalized Rabi frequency, in addition to the central peak. The spectra are very sensitive to the details of the spectrum of the frequency fluctuations of the input laser field. For strong fields, the spectra are also quite sensitive to the spatial-intensity distribution across the interaction region. For driving fields with a finite bandwidth of the phase fluctuations (leading to a non-Lorentzian laser spectrum) the peaks at the Rabi frequency are significantly reduced. These observations are consistent with the predictions of Ritsch, Zoller, and Cooper.[3] Asymmetric variance profiles have been observed for correlated amplitude and frequency noise on the input laser field.

ACKNOWLEDGMENTS

We are grateful to J. L. Hall, D. Z. Anderson, and those cited in Ref. 1 for useful conversations. We are also grateful to A. Maquet for assistance in the numerical analysis. This work was supported in part by the U.S. Department of Energy, Office of Basic Energy Sciences. One of us (J.C.) was supported by the National Science Foundation, Grant No. PHY 86-04504.

[1]C. W. Wieman, C. Tanner, and L. Hollberg (private communication).

[2]Th. Haslwanter, H. Ritsch, J. Cooper, and P. Zoller, Phys. Rev. A **38**, 5652 (1988).

[3]H. Ritsch, P. Zoller, and J. Cooper, Phys. Rev. A **41**, 2653 (1990).

[4]M. H. Anderson, R. D. Jones, J. Cooper, S. J. Smith, D. S. Elliott, H. Ritsch, and P. Zoller, Phys. Rev. Lett. **64**, 1346 (1990).

[5]H. J. Kimble, M. Dagenais, and L. Mandel, Phys. Rev. A **18**, 201 (1978).

[6]K. Wódkiewicz, Phys. Lett. **77A**, 315 (1980); J. Phys. B **14**, L529 (1981); H. J. Kimble and L. Mandel, Phys. Rev. A **15**, 689 (1977); G. S. Agarwal, Phys. Rev. Lett. **37**, 1387 (1976).

[7]K. Rzazewski, B. Stone, and M. Wilkens, Phys. Rev. A **40**, 2788 (1989).

[8]B. A. Ferguson and D. S. Elliott, Phys. Rev. A **41**, 6183 (1990).

[9]M. W. Hamilton (private communication).

[10]M. W. Hamilton, K. Arnett, S. J. Smith, D. S. Elliott, M. Dziemballa, and P. Zoller, Phys. Rev. A **36**, 178 (1987).

[11]K. Arnett, S. J. Smith, R. E. Ryan, T. Bergeman, H. Metcalf, M. W. Hamilton, and J. R. Bradenberger, Phys. Rev. A **41**, 2580 (1990).

[12]N. Morita and T. Yajima, Phys. Rev. A **30**, 2525 (1984).

[13]R. Trebino, E. D. Gustafson, and A. E. Siegman, J. Opt. Soc. Am. B **3**, 1295 (1985).

[14]D. S. Elliott, M. W. Hamilton, K. Arnett, and S. J. Smith, Phys. Rev. A **32**, 887 (1985).

[15]R. Boscaino and R. N. Mantegna, Opt. Commun. **73**, 289 (1989).

[16]J. E. Golub, Y. S. Bai, and T. W. Mossberg, Phys. Rev. A **37**, 119 (1988).

[17]P. L. Knight, W. Molander, and C. R. Stroud, Phys. Rev. A **17**, 1547 (1978).

[18]S. N. Dixit, P. Zoller, and P. Lambropoulos, Phys. Rev. A **21**, 1289 (1989).

[19]D. S. Elliott and S. J. Smith, J. Opt. Soc. Am. B **5**, 1927 (1988).

[20]R. E. Grove, F. Y. Wu, and S. Ezekiel, Phys. Rev. A **15**, 227 (1977).

[21]L. Westling (private communication), L. Hollberg has observed similar asymmetries in the fluctuations of fluorescence from cesium atoms driven by stabilized diode lasers.